Proceedings of the 21st International Conference on Automation & Computing, University of Strathclyde, Glasgow, UK, 11-12 September 2015

A Study of Diagnostic Signatures of a Deep Groove Ball Bearing Based on a Nonlinear Dynamic Model

Ibrahim Rehab, Xiange Tian, Fengshou Gu and Andrew D. Ball
Centre for Efficiency and Performance Engineering,
University of Huddersfield, Huddersfield, UK

***Abstract*— For accurate fault detection and diagnosis, this paper focuses on the study of bearing vibration responses under increasing radial clearances due to investable wear and different bearing grades. A nonlinear dynamic model incorporating with local defects and clearance increments is developed for a deep groove ball bearing. The model treats the inner race-shaft and outer race-housing as two lumped masses which are coupled by a nonlinear spring formalized by the Hertzian contact deformation between the balls and races. The solution of the nonlinear equation is obtained by a Runge-Kutta method in Matlab. The results show that the vibrations at fault characteristic frequencies exhibit significant changes with increasing clearances. However, an increased vibration is found for the outer race fault whereas a decreased vibration is found for inner race fault. Therefore, it is necessary to take into account these changes in determining the size of faults.**

Keywords- radial clearance; contact deformation; condition monitoring; bearing defects

I. INTRODUCTION

A large number of papers have been focused on developing signal processing techniques to detect and isolate faults of bearings with high degree of accuracy. But relatively few studies have presented a mathematical (physics-based) model, where faults can be simulated under different operating conditions rather than waiting for their natural occurrence, or alternatively having them seeded for laboratory testing.

Different mathematical models have been developed to study the dynamic effects on the roller bearing. In 1984, McFadden and Smith developed a model which described the vibration produced by a single point defect on the inner race of a rolling element bearing under constant radial load [1]. Purohit et al. (2006) [2] studied the radial and axial vibrations of a rigid shaft supported ball bearing. In the analytical formulation the contacts between the balls and the races are considered as nonlinear springs, whose stiffness is obtained by using the Hertzian elastic contact deformation theory. Culita et al. (2007) [3] presented the McFadden- Smith vibration model, one of the first valid models of vibration generated by single point defects in bearings. They presented how the defect is encoded by vibration in a more accurate and natural manner than previous models. A significant important contribution was brought by S. Sassi et al. (2007) [4]. They developed a numerical model with the assumption that the dynamic behavior of the bearing can be represented by a coupled three-degree-of-freedom system. Upadhyan et al. (2009) [5] studied the dynamic behavior of a high speed unbalanced rotor supported on roller bearings with damping. The non-linearity in the rotor bearing system has been considered mainly due to Hertzian contact, unbalanced rotor effect and radial internal clearance. Patil et al. (2010) [6] presented an analytical model for predicting the effect of a localized defect on the ball bearing vibrations. In the analytical formulation, the contacts between the ball and the races are considered as non-linear springs. Dougdag et al. (2012) [7] presented an experimental verification of a simplified model of a nonlinear stiffness ball bearing in both static and dynamic modes and tested its capabilities to simulate accurately fault effects. Results of defects simulation and model behavior in statics and dynamics are compared to experimental results. Patel et al. (2013) [8] reported a theoretical and experimental vibration study of dynamically loaded deep groove ball bearings having local circular shape defects. The shaft, housing, raceways and ball masses are incorporated in the proposed mathematical model. Coupled solutions of governing equations of motion had been achieved using Runge-Kutta method.

The objective of this paper is to develop a relatively more realistic dynamic model of deep grove ball bearing in presence of different internal radial clearances and localized defects.

II. DYNAMIC MODEL WITH BEARING DEFECTS

A single ball bearing consists of a number of parts. The description of each component can lead to a simulation model with a large number of degrees of freedom (DOF). The free body diagram of the shaft bearing system is provided in Fig. 1. Moreover, the deep grove ball bearing (6206) is the studied bearing. The model of the study bearing system is carried out using springs and lumped masses. The proposed model incorporates the following realistic assumptions and considerations.

- Balls are positioned equi-spaced balls around the shaft and there is no interaction between them.
- There is no slipping of the balls during rolling on the surface of races.
- The mass of the ball is negligible because it is relatively small compared with other bearing parts refer to the Table I.

- The study bearing operates under isothermal conditions.
- Forces act in radial directions along X and Y axes.
- The mass of the inner race is included in the mass of the shaft, and the mass of the housing incorporates the mass of the outer race.
- The shaft-housing under study is modelled using two masses (M_s and M_h), which yields a 2-DOF system.
- Nonlinear Hertzian contact deformations are considered at the contacts formed between balls and races.
- Damping due to lubricant film is ignored.

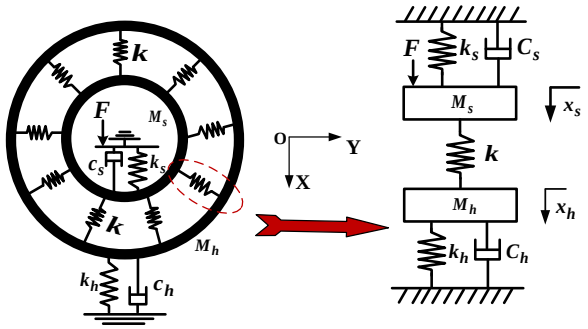

Figure 1. Free body diagram of the shaft-housing system

The geometric and physical properties of the studied bearing are presented in Table I.

TABLE I. GEOMETRIC AND PHYSICAL PROPERTIES USED FOR THE BALL BEARINGS

Geometric properties			Physical properties		
Symbol	*value*	*Unit*	*Symbol*	*value*	*Unit*
d_s	30	mm	E	210	KN/mm^2
d_i	37.48	mm	ν	0.3	-
d_o	56.45	mm	M_o	59.84	g
d_m	46.96	mm	M_i	32.4	g
D	9.48	mm	M_b	2.95	g
p_d	0.01	mm	M_s	5.26	Kg
N_b	9	-	M_h	1	Kg

where M_o, M_i, M_b, M_s and M_h are the masses of outer race, inner race, ball, shaft and housing respectively.

A. Load Deflection and Stiffness

Hertzian load deformation relationship is used in calculation of deformation at the contacts formed between ball and races of the bearing under investigation. The used relation is expressed as the following [9]:

$$Q = K\delta^n \tag{1}$$

where K is the load deflection factor or constant for Hertzian contact elastic deformation, δ is the radial deflection or contact deformation and n is the load deflection exponent, $n = 3/2$ for ball bearing and $10/9$ for roller bearing [9].

The stiffness coefficient at the contacts formed between races and the *ith* ball are evaluated using the following relation [10, 11]:

$$K_{i,o} = \frac{2\sqrt{2}\left(\frac{E}{1-\nu^2}\right)}{3\left(\sum\rho\right)^{1/2}}\left(\frac{1}{\delta^*}\right)^{3/2} \tag{2}$$

where $K_{i,o}$ is inner and outer raceways to ball contact stiffness respectively, $\sum\rho$ is the curvature sum which is calculated using the radii of curvature in a pair of principal planes passing through the point contact. δ^* is the dimensionless contact deflection obtained using curvature difference (Refer Table 6.1, Rolling Bearing Analysis, Tedric Harris, Fourth Edition, 2001).

Total deflection between two raceways is the sum of the approaches between the rolling elements and each raceway [9], hence,

$$K = \left[\frac{1}{(1/K_i)^{1/(3/2)} + (1/K_o)^{1/(3/2)}}\right]^{3/2} \tag{3}$$

Fig. 2 shows the rigidly supported bearing subjected to radial load, the radial deflection at any rolling element angular position is given by [9]:

$$\delta_\phi = \delta_r \cos\phi - \frac{1}{2}P_d \tag{4}$$

where δ_r is the ring radial shift, occurring at $\phi = 0$ and P_d is the diametric clearance.

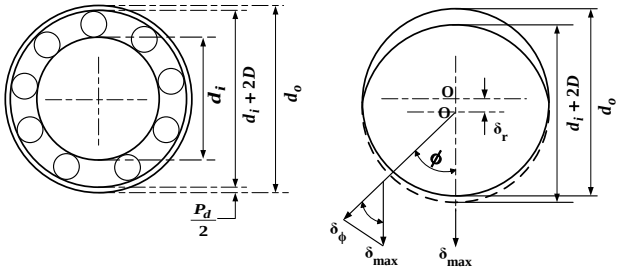

Figure 2. Radial deflection at a rolling element position [9]

If ϕ_0 is the initial position of the *ith* ball, the angular position ϕ_i at any time t is defined by the following relation:

$$\phi_i = \frac{2\pi}{N_b}(i-1) + \omega_c t + \phi_0\,,\ i = 1,...,N_b \tag{5}$$

where the angular velocity ω_c of the cage can be expressed in terms of angular velocity ω_s of the shaft as:

$$\omega_c = \left(1 - \frac{D}{d_m}\right)\frac{\omega_s}{2}\,,\ \omega_s = 2\pi f_s \tag{6}$$

The radial deflection at any rolling element angular position may be rearranged in terms of maximum deformation as follows:

$$\delta_\phi = \delta_{\max}\left[1 - \frac{1}{2\varepsilon}(1 - \cos\phi_i)\right] \tag{7}$$

where $\varepsilon = \frac{1}{2}\left(1 - \frac{P_d}{2\delta_r}\right)$

Therefore, the contact force at any angular position is

$$Q_\phi = Q_{\max}\left[1 - \frac{1}{2\varepsilon}\left(1 - \cos\phi_i\right)\right]^{3/2} \quad (8)$$

In Fig. 3 it is clear that the overall applied radial load (F) is equal to the sum of the vertical components of the contact reactions of the rolling element loads. Mathematically, it is expressed as follows:

$$F = \sum_{\phi=0}^{\phi=\pm\psi_I} Q_\phi \cos\phi \quad (9)$$

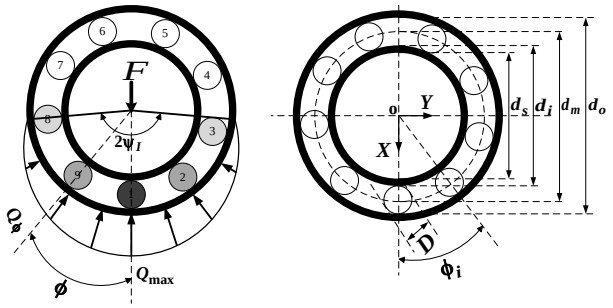

Figure 3. Load distributions in a ball bearing

The overall contact deformation δ for the *ith* ball is a function of the shaft displacement relative to the housing in the radial direction, ball position ϕ_i and the clearance c is provided by following expression.

$$\delta = \left(X_s - X_h\right)\cos\phi_i + \left(Y_s - Y_h\right)\sin\phi_i - c \quad (10)$$

where $c = P_d/2\left(1 - \cos\phi_i\right)$ is the internal radial clearance.

Since the Hertzian forces arise only when there is a contact deformation, the springs are required to act only in compression. In other words, the respective spring force comes into play when the instantaneous spring length is shorter than its unstressed length (the terms of δ should be positive), otherwise the separation between ball and race takes place and the restoring force is set to zero.

At the time of impact at the defect, a pulse of short duration is produced and it is accounted for by the term Δ additional deflection. Hence the expressions for δ is modified as:

$$\delta = \left(X_s - X_h\right)\cos\phi_i + \left(Y_s - Y_h\right)\sin\phi_i - c - \Delta \quad (11)$$

The total restoring force is the sum of the restoring force from each of the rolling elements. Thus the total restoring force components in the X and Y directions are

$$F_X = \sum_{i=1}^{N_b} K\left[\delta\right]^{3/2}\cos\phi_i \quad (12)$$

$$F_Y = \sum_{i=1}^{N_b} K\left[\delta\right]^{3/2}\sin\phi_i \quad (13)$$

B. Internal Clearance

Internal radial clearance is the geometrical clearance between the inner race, outer race and ball. Radial clearance is the play between the ball and raceway perpendicular with the bearing axis. The internal clearance will significantly influence heat, vibration, noise, and fatigue life. For best rolling element bearing life and machine reliability, internal clearance at running conditions must be close to zero [9, 12]. Moreover, it is also necessary for the purpose of diagnosis to gain the knowledge of changes on the characteristic features when the clearance becomes large due to investable wear during the bearing service life.

The angular contact ball bearings are specifically designed to operate under radial and thrust load, and the clearance built into the unloaded bearing angle. In addition, there are five clearance groups, namely C2, C0 (Normal), C3, C4 and C5. Therefore, the radial internal clearances for radial contact deep groove ball bearing (6206) are presented in Table II [9].

TABLE II. RADIAL INTERNAL CLEARANCE FOR DEEP GROOVE BALL BEARING 6206 UNDER NO LOAD [ISO 5753]

Clearance values (μm)									
C2		***C0***		***C3***		***C4***		***C5***	
Min	***Max***	***Min***	***Max***	***Min***	***Max***	***Min***	***Max***	***Min***	***Max***
1	11	6	20	15	33	28	46	40	64

C. Equation of Motion

Based on the assumption made, the governing equations for each mass in shaft and housing in X and Y directions can be developed. According to the motion direction in Fig. 1, the equations are:

$$M_s\ddot{X}_s + C_s\dot{X}_s + K_sX_s + \sum_{i=1}^{N_b} K\left[\delta\right]^{3/2}\cos\phi_i + F = 0 \quad (14)$$

$$M_s\ddot{Y}_s + C_s\dot{Y}_s + K_sY_s + \sum_{i=1}^{N_b} K\left[\delta\right]^{3/2}\sin\phi_i = 0 \quad (15)$$

$$M_h\ddot{X}_h + C_h\dot{X}_h + K_hX_h - \sum_{i=1}^{N_b} K\left[\delta\right]^{3/2}\cos\phi_i = 0 \quad (16)$$

$$M_h\ddot{Y}_h + C_h\dot{Y}_h + K_hY_h - \sum_{i=1}^{N_b} K\left[\delta\right]^{3/2}\sin\phi_i = 0 \quad (17)$$

D. Local Defect

1) Defect on the Inner Race

The location of defects on the inner race does not remain stationary since the inner race rotates at the speed of the shaft ω_s. Thus, the defect angle for the inner race α_{in} is defined as:

$$\alpha_{in} = \omega_s t \pm \left(W_{defect}/d_i\right) \quad (18)$$

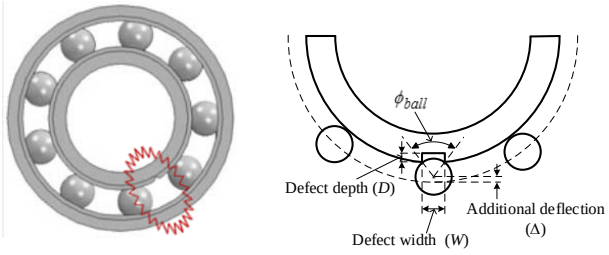

Figure 4. Additional deflection of ball due to defect on inner race

The rolling ball approaches the defect either in the loaded zone or the unloaded zone, therefore, the deflection δ of the *ith* ball varies. Additional deflection at the defect Δ of the ball when it passes through the defect is defined by the width of the defect as following:

$$\Delta = \left(D/2 - D/2 * \cos(0.5\phi_{ball})\right) \quad (19)$$

where ϕ_{ball} = width of the defect / radius of the ball.

The position of the *ith* ball in the defect zone is mathematically defined as:

$$\left(\omega_s t - W_{defect}/d_i\right) \le \phi_i \le \left(\omega_s t + W_{defect}/d_i\right) \quad (20)$$

2) Defect on the Outer Race

The defect on the outer race is located at an angle α_{out} from the *X* axis. The local defects on the outer race are normally found in the loaded region. Moreover, the stationary outer race means that the position of the defect usually does not change. Whenever a ball passes over the defect location, it has additional deflection Δ.

The angular position of *ith* ball passing the defect zone is mathematically defined by the following relation:

$$\left(\alpha_{out} - W_{defect}/d_o\right) \le \phi_i \le \left(\alpha_{out} + W_{defect}/d_o\right) \quad (21)$$

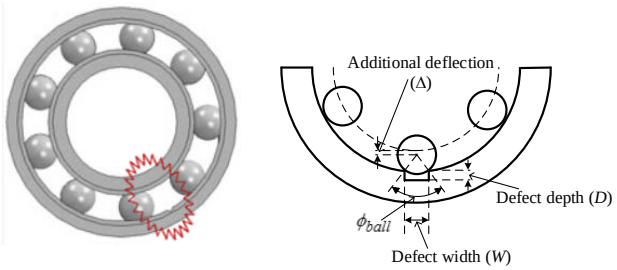

Figure 5. Additional deflection of ball due to defect on outer race

III. Diagnostic Features with Clearance

The above equations (14-17) are second order nonlinear differential equations. To solve these equations each of the second order equations is converted into two first order differential equations. The Runge-Kutta method is used to solve the first differential equation set in Matlab environment.

A. Initial Conditions

The governing equations of motion are solved based on the ball positions (5) and the deflection relation (11) at each step of time. Displacement in *X* and *Y* directions and velocity $\dot{X}$ and $\dot{Y}$ at time $(t + dt)$ are calculated. The time step (dt) of 6 μs for nine cycles has been considered. The initial displacements and velocities in *X* and *Y* directions are set to zeroes.

The shaft speed of 1500 rpm (25 Hz) with 1000 N radial load is considered as the normal operating condition of the bearing. Two defect sizes with width 0.6 mm and 2.0 mm on both the inner race and outer race will be studied subsequently, which are denoted as small and large faults respectively. The details of the calculation process are summarized in the flow chart of Fig. 6.

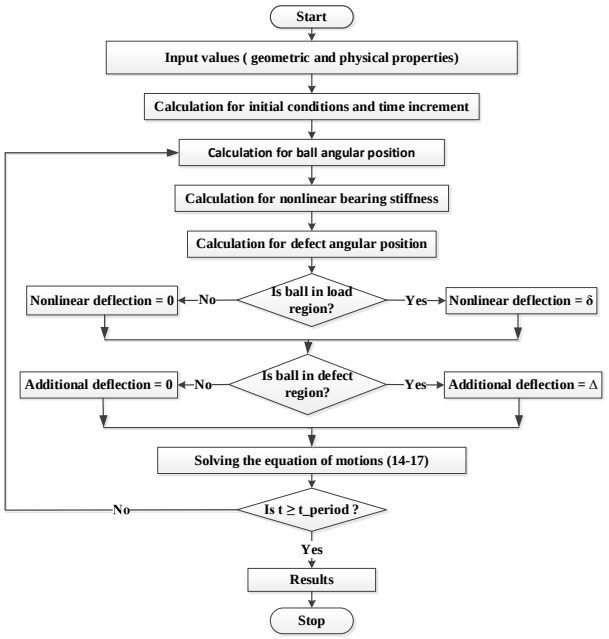

Figure 6. The flow chart of calculation process

B. Diagnosis of Outer Race Defect

The defect on outer race often occurs in loading zone and will have a constant angular position, usually corresponding to the applied direction of the external loading. Therefore, when a moving ball approaches to the defect same magnitude of impulse is expected for every time of contact between ball and defect. On the other hand, the defect my also appear at the start of loading zone due to poor lubricant conditions. Therefore, two outer race defect locations (0 degree and 320 degrees) have been examined for two defect widths 0.6 mm and 2.0 mm under four incremental different clearance values 1, 10, 30 and 60 μm.

1) Outer Race Defect at 0 Degree

Fig. 7 presents vibration displacements of the housing in X direction for baseline, small defect and large defect when the clearance values are at 1, 10, 30 and 60 μm. It can be seen that the baseline case, where is no defect on the races, exhibit a clear increase in vibration displacement with clearance increments, showing that the amplitude of local becomes higher with larger clearances. Moreover, for the two defect cases, the periodic vibration amplitudes also show significant increases with clearances and large defect have higher amplitudes.

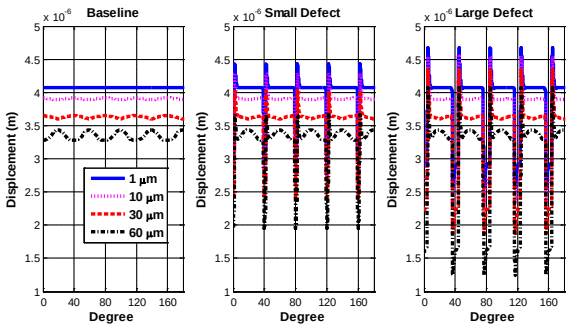

Figure 7. Housing displacements in X direction

To show the impact behavior, Fig. 8 shows the vibration velocities of housing in X direction of baseline, small defect and large defect at four different clearance values. For the baseline case, clear increase in vibration velocity amplitude can be seen as result of clearance increases. For the defect case, the impulse caused by the contact between ball and defect is repeated each 40 degrees. Moreover, both the impulse magnitude and duration increase with the defect size.

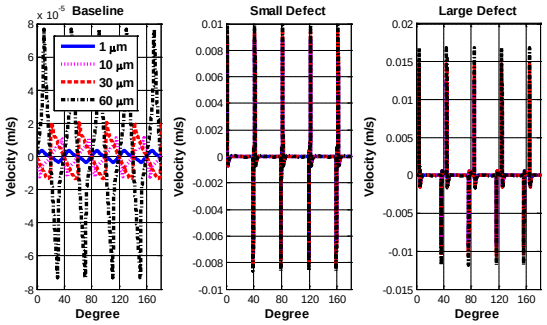

Figure 8. Housing velocities in x direction

The frequency spectra of housing acceleration in X direction of baseline, small defect and large defect cases are illustrated in Fig. 9. For the baseline the loading frequency which is the cage frequency multiply by the number of balls can be clearly appeared. For the defect case, the calculated ball pass frequency outer race (BPFO) is 89.8Hz. The fault feature frequency and its harmonics are obviously obtained. Moreover, the increase of the defect acceleration magnitude is caused by the defect size and nonlinear deflection.

$$BPFO = \frac{N_b}{2} F_s \left(1 - \frac{D}{d_m} \cos\phi\right) \tag{22}$$

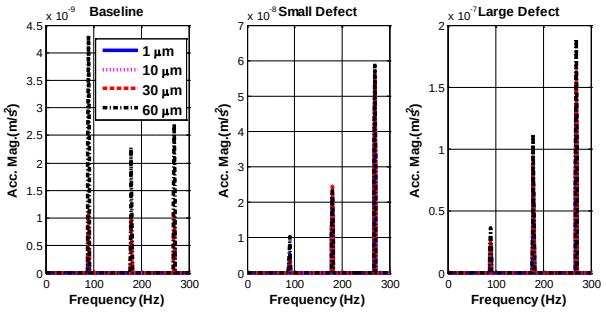

Figure 9. Housing acceleration spectrum in X direction

The acceleration amplitudes of housing in X direction of baseline, small defect and large defect cases are shown in Fig. 10. For the baseline case, the loading frequency amplitude is increased owing to large clearances. For the defect case, the BPFO magnitude and its harmonics are increasing with the increase of the clearance values. Additionally, the magnitude of the BPFO of the small defect is greatly affected by the loading frequency.

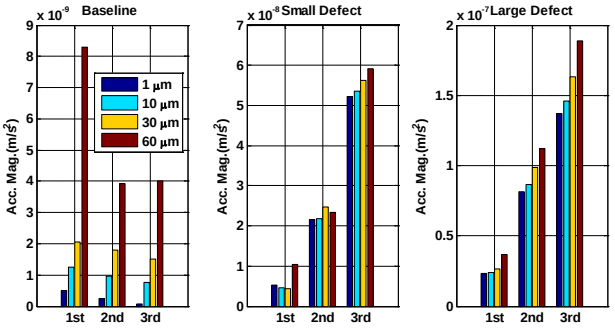

Figure 10. Acceleration amplitude on house of first three harmonics of fault characteristic frequency

2) Outer Race Defect at 320 Degrees

The vibration acceleration amplitudes of defective outer race at 320 degrees in X direction of small defect and large defect cases are shown in Fig. 11. The magnitude of the BPFO is greatly affected by the loading frequency. Furthermore, the BPFO magnitude and its harmonics are decreased with the increase of the clearance values.

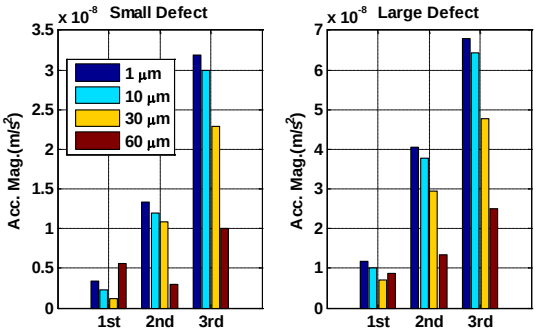

Figure 11. Acceleration amplitude on house of first three harmonics of fault characteristic frequency

The vibration acceleration amplitudes of different position of outer race defect show significant changes. When the defect is at 0 degree, the amplitude of vibration is maximum. As the position of the defect is changed away from this position, it is observed that the amplitude of vibration reduces. This variation can be seen in Fig. 10 and Fig. 11.

C. Diagnosis of Inner Race Defect

Rotating inner race defect generates a complicated vibration signal due to rotation of both defect and balls. The amplitude of the inner race defect is not constant due to the varying load on ball and defect contacts.

Vibration displacements of the housing in X direction at four different clearance values of small defect and large defect cases are presented in Fig. 12. As the rolling ball approaches the defect either in the loaded zone or the unloaded zone the periodic vibration amplitudes show significant variation.

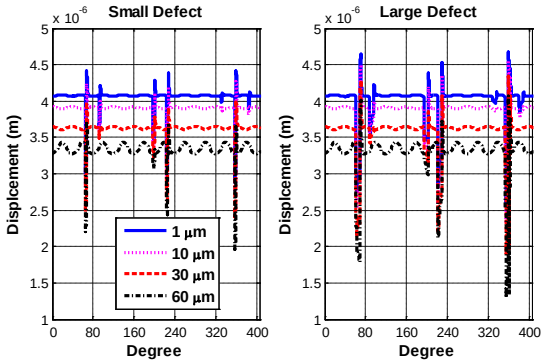

Figure 12. Housing displacements in X direction

The housing vibration velocities in X direction of small defect and large defect cases are presented in Fig. 13. It is clearly indicated that the velocity magnitude increases when the defect and ball contact accrue in the load zone and decrease in the unloaded zone.

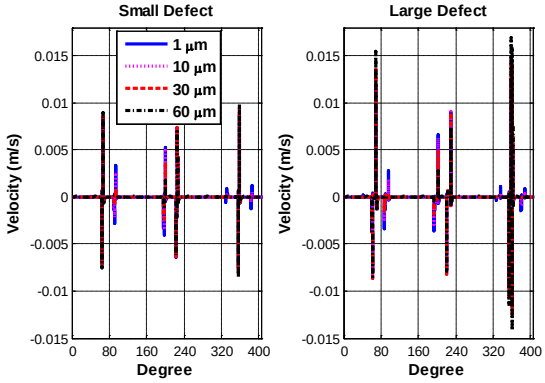

Figure 13. Housing velocities in X direction

The frequency spectra of housing vibration in X direction of small defect and large defect cases are shown in Fig. 14. The calculated ball pass frequency inner race (BPFI) is 135.198 Hz. The fault feature frequency and shaft rotational frequency and their harmonics are clearly visible. Furthermore, the inner race defect rotates at shaft speed, so the *BPFI* is amplitude modulated by the shaft rotational frequency. Therefore, peaks at frequencies $BPFI \pm f_s$ and their harmonics are also found.

$$BPFI = \frac{N_b}{2} F_s (1 + \frac{D}{d_m} \cos\phi) \qquad (24)$$

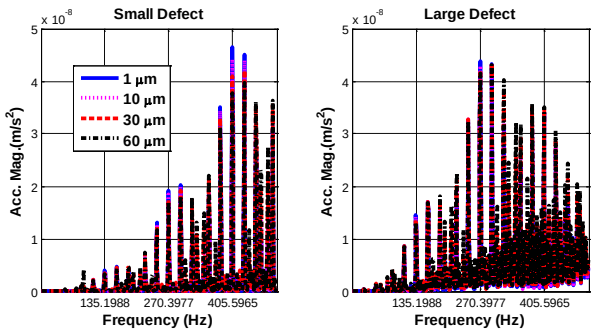

Figure 14. Housing acceleration spectrum in X direction

The acceleration amplitudes of small and large inner race defect cases are presented in Fig. 15. The defect amplitude is decreasing with the increase of the clearance value. For the large defect, the third harmonic amplitude is greatly affected by the system frequency response.

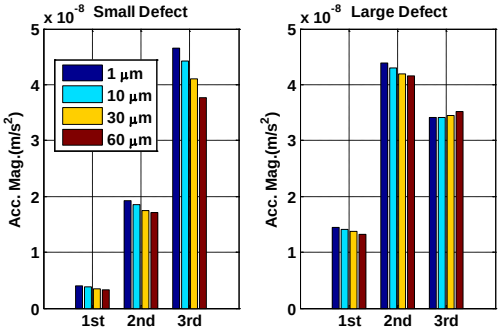

Figure 15. Acceleration amplitude on house of first three harmonics of fault characteristic frequency

IV. Conclusion

A dynamic model for deep groove ball bearings considering internal radial clearance as well as localized defects on inner and outer races is developed to obtain the vibration responses for bearing diagnosis. The bearing is modelled as a 2-DOF system, vibrations of shaft and housing in X and Y directions are studied. The vibration acceleration amplitudes and frequencies are simulated by solving the coupled nonlinear equation of motions using Matlab.

The model predicts that the vibration responses increase with internal radial clearances which will become large during bearing service period due to inevitable wear. As expected, the large the clearance the higher amplitude of the diagnostic feature for the outer race defects. In addition, the defect at loading zone produces higher amplitude.

However, the large clearance reduces the amplitudes of the feature for inner race defects. Therefore, the severity of inner race fault needs to be determined by taking into account bearing service duration and bearing grades.

References

1. McFadden, P.D. and J.D. Smith, *Model for the vibration produced by a single point defect in a rolling element bearing.* Journal of Sound and Vibration, 1984. 96(1): p. 69-82.
2. Purohit, R. and K. Purohit, *Dynamic analysis of ball bearings with effect of preload and number of balls.* International Journal of Applied Mechanics and Engineering, 2006. 11(1): p. 77-91.
3. Culita, J., D. Stefanoiu, and F. Ionescu, *Simulation models of defect encoding vibrations.* Journal of Control Engineering and Applied Informatics, 2007. 9(2): p. 59-67.
4. Sassi, S., B. Badri, and M. Thomas, *A numerical model to predict damaged bearing vibrations.* Journal of Vibration and Control, 2007. 13(11): p. 1603-1628.

5. Upadhyay, S., S. Harsha, and S. Jain, *Analysis of nonlinear phenomena in high speed ball bearings due to radial clearance and unbalanced rotor effects.* Journal of Vibration and Control, 2010. 16(1): p. 65-88.
6. Patil, M.S., et al., *A theoretical model to predict the effect of localized defect on vibrations associated with ball bearing.* International Journal of Mechanical Sciences, 2010. 52(9): p. 1193-1201.
7. Dougdag, M., et al., *An experimental testing of a simplified model of a ball bearing: stiffness calculation and defect simulation.* Meccanica, 2012. 47(2): p. 335-354.
8. Patel, V.N., N. Tandon, and R.K. Pandey, *Vibration Studies of Dynamically Loaded Deep Groove Ball Bearings in Presence of Local Defects on Races.* Procedia Engineering, 2013. 64(0): p. 1582-1591.
9. Harris, T.A. and M.N. Kotzalas, *Rolling Bearing Analysis, Fifth Edition - 2 Volume Set*. 2006: Taylor & Francis.
10. Arslan, H. and N. Aktürk, *An investigation of rolling element vibrations caused by local defects.* Journal of Tribology, 2008. 130(4): p. 041101.
11. Karacay, T. and N. Akturk, *Vibrations of a grinding spindle supported by angular contact ball bearings.* Proceedings of the Institution of Mechanical Engineers, Part K: Journal of Multi-body Dynamics, 2008. 222(1): p. 61-75.
12. Oswald, F.B., E.V. Zaretsky, and J.V. Poplawski, *Effect of Internal Clearance on Load Distribution and Life of Radially Loaded Ball and Roller Bearings.* Tribology Transactions, 2012. 55(2): p. 245-265.